Radiology

Photoacoustic Imaging in Oncology: Translational Preclinical and Early Clinical Experience[1]

Keerthi S. Valluru, BTech, MS
Katheryne E. Wilson, PhD
Jürgen K. Willmann, MD

Photoacoustic imaging has evolved into a clinically translatable platform with the potential to complement existing imaging techniques for the management of cancer, including detection, characterization, prognosis, and treatment monitoring. In photoacoustic imaging, tissue is optically excited to produce ultrasonographic images that represent a spatial map of optical absorption of endogenous constituents such as hemoglobin, fat, melanin, and water or exogenous contrast agents such as dyes and nanoparticles. It can therefore provide functional and molecular information that allows noninvasive soft-tissue characterization. Photoacoustic imaging has matured over the years and is currently being translated into the clinic with various clinical studies underway. In this review, the current state of photoacoustic imaging is presented, including techniques and instrumentation, followed by a discussion of potential clinical applications of this technique for the detection and management of cancer.

©RSNA, 2016

Radiology

The fundamental principle behind medical imaging is to noninvasively depict an underlying tissue property based on the interaction of tissue with some form of radiation. Photoacoustic (interchangeably "optoacoustic") imaging creates light-induced ultrasonographic (US) images to illustrate tissue optical absorption.

Essentials

- Photoacoustic imaging creates light-induced US images to illustrate tissue optical absorption and allows safe, cost-effective, real-time image acquisition to convey underlying physiologic information of the tissue.

- Photoacoustic signal generation depends on laser parameters, while photoacoustic signal detection and image formation rely on US imaging principles.

- Spectroscopic photoacoustic imaging is a powerful technique that can detect variations in the concentration of endogenous tissue constituents such as oxygenated hemoglobin, which have unique optical absorption properties and facilitate the differentiation of cancer from surrounding tissue.

- Currently, photoacoustic imaging instrumentation is commercially available only for preclinical studies; with a few clinical trials underway, clinical photoacoustic imaging systems are gearing toward regulatory approval for commercial adoption in the United States.

- Photoacoustic imaging systems come in a variety of configurations ranging from completely custom-developed systems to integrated clinical US scanners for clinical applications and could lead to earlier detection and better characterization of several cancer types, including breast cancer, prostate cancer, skin cancer, thyroid cancer, ovarian cancer, and cervical cancer.

Since many of the primary constituents of tissue, including water, hemoglobin, lipids, and collagen, have unique optical absorption spectra, photoacoustic imaging performed over multiple wavelengths (spectroscopic imaging) can detect variations in the concentration of these tissue components in cancer and surrounding tissue. Furthermore, exogenous contrast agents can facilitate molecular photoacoustic imaging by specifically targeting cancer biomarkers. With primary advantages including clinically relevant imaging depths up to 7 cm with submillimeter resolution (1), high contrast-to-noise ratios (up to 100) attributed to spectroscopic imaging (2), real-time acquisition, portability, lack of ionizing radiation exposure, and ease of integration into existing clinical US scanners, photoacoustic imaging holds promise as a clinically translatable modality for cancer detection. Currently, several clinical applications of photoacoustic imaging are being explored in clinical trials, including imaging of breast, prostate, and ovarian cancer, as well as other tissues. In this review, the general principles of photoacoustic imaging are presented followed by a discussion about potential clinical applications pertaining to cancer imaging.

General Principles of Photoacoustic Imaging

Photoacoustic Effect

The photoacoustic effect, the conversion of light to sound, was first described by Bell in the late 1800s (3). Since then, researchers have spent the past decades exploring this principle for medical imaging purposes (4–7). Typically, photoacoustic imaging uses nanosecond pulses of laser light to irradiate tissues, where tissue constituents absorb the light creating localized heating and rapid thermal expansion of the surrounding environment (Fig 1). This thermal expansion, upon contraction to the original state, releases high-frequency and broad-band acoustic transients (high-amplitude, short-duration waves), which propagate from the absorber as spherical waves that can be detected and reconstructed by using standard US equipment and algorithms (4,8).

Photoacoustic Signal Generation

The primary component required to generate photoacoustic signals within tissue is a high-energy pulsed laser. The choice of wavelengths depends on the targeted application and can range from ultraviolet to infrared, with maximum tissue penetration achievable in the near-infrared spectrum of 700–1100 nm (9,10). The laser pulse duration is an important factor affecting photoacoustic image quality. Shorter pulse widths, typically less than 10 nsec, achieve both stress and thermal confinement conditions required of photoacoustic imaging. Stress confinement is fulfilled when the laser pulse is substantially shorter than the stress relaxation time of the environment, while thermal confinement condition is satisfied when the laser pulse duration is shorter than the thermal relaxation time. These conditions ensure that high-frequency photoacoustic transients are generated as relative point sources of optical absorption event (11). Furthermore, high laser fluence, which is the energy delivered per unit area (units: J/cm^2), yields increased photoacoustic transient production in tissue and better imaging depth. To ensure patient safety, maximum permissible exposure limits are set (for the skin, 20–100 mJ/cm^2 at 700–1050 nm) (12). Furthermore, high pulse repetition rates allow "real-time" photoacoustic image acquisition (the typical US image acquisition rates range between approximately 1 and 10 kHz for clinical scanners [13]). Currently, most photoacoustic imaging systems use solid-state (Q-switched) lasers,
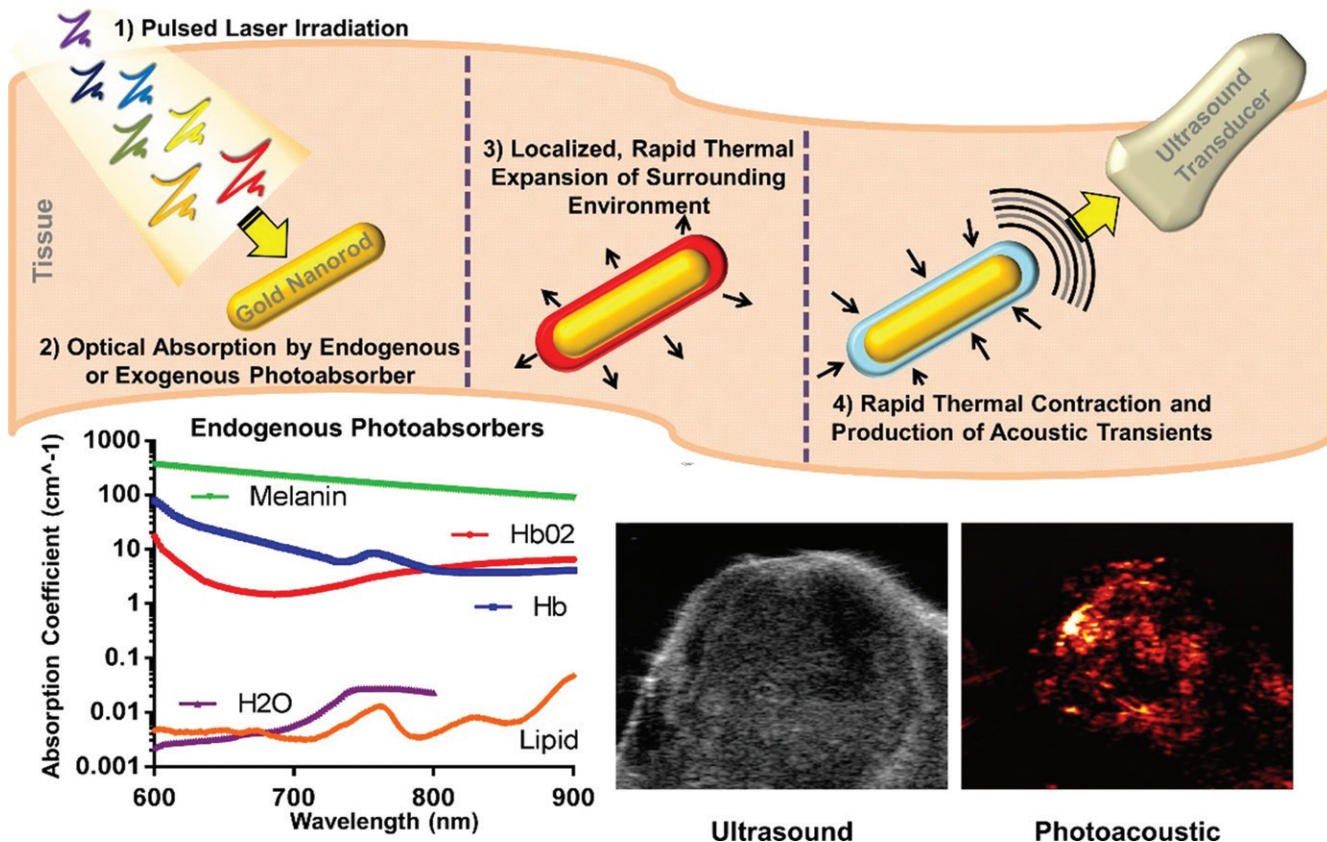
Figure 1: Top: Illustration of the photoacoustic effect. Pulsed laser irradiation is absorbed by either a contrast agent or endogenous tissue chromophore. Energy deposition is sufficiently fast to prevent diffusion and allow for a localized and rapid thermal expansion of the environment immediately surrounding the chromophore. With the cooling and contraction of the environment, high-frequency and broadband acoustic transients are released. These transients can be detected with a standard US transducer. Bottom left: Absorption spectra of endogenous chromophores in near-infrared region are shown including melanin (limited to skin) and oxygenated *(HbO2)* and deoxygenated hemoglobin *(Hb)* (the primary chromophores in tissue); water and lipid have significantly lower absorption coefficients in the near-infrared range. Bottom right: An example of a coregistered US and photoacoustic image showing a map of optical absorption primarily from hemoglobin in a mouse tumor. Brighter signals in photoacoustic image correspond to stronger optical absorption and are not correlated with the intensity of the anatomic image provided with B-mode US.

but are limited to repetition rates less than tens of hertz. Fast diode lasers triggering at kilohertz rates allow real-time acquisition but have longer pulse widths and yield lower fluence, making them impractical for clinical applications.

Photoacoustic Signal Detection

A US transducer array that is placed on the surface of the illuminated region can only detect a portion of the spherical photoacoustic transients. Alternatively, a photoacoustic computed tomographic (CT) approach can acquire a majority of the photoacoustic transients, increasing signal-to-noise ratio and improving image quality (14). Typically, photoacoustic signals from biologic absorbers contain frequencies in the range of 1–10 MHz (15), and a broadband US transducer fabricated with polyvinylidene fluoride is more appropriate for photoacoustic imaging compared with lead zirconate titanate transducers conventionally used in clinical US systems (16).

Photoacoustic Image Formation

For photoacoustic imaging systems integrated with clinical US scanners, the same onboard processing approaches

(logarithmic compression, time gain compensation, delay and sum algorithms, etc) apply to photoacoustic image formation. In the aforementioned photoacoustic CT approach, photoacoustic signals from all the transducer elements are filtered, back projected, and added to reconstruct an image similar to a CT scan (17). Since photoacoustic CT imaging requires custom transducer arrangement, which in turn leads to a dedicated photoacoustic imaging system, greater control over photoacoustic data acquisition can be exercised and time-dependent radiofrequency (containing amplitude, phase,

and frequency) data can be extracted, allowing more precise image quantification. Typically, the photoacoustic signal amplitude is proportional to the absorbed laser energy at any given location, while the differences in tissue optical absorption dictate image contrast. The image resolution depends on various factors: *(a)* Lateral resolution is determined by the frequency response and the width of the transducer element (without any focusing, a wider transducer will yield high signal-to-noise ratio and high detection sensitivity but lower lateral resolution); *(b)* axial resolution is determined by the frequency of the photoacoustic signal generated from the absorber (unlike in conventional US, where spatial pulse length or frequency of the excitation beam dictates axial resolution); and *(c)* elevational resolution (section thickness) depends on the height of the transducer element and is important in the context of three-dimensional volumetric imaging.

Photoacoustic Spectroscopy

Photoacoustic imaging is inherently a molecular imaging modality as optical absorption is dependent on the molecular structure of chromophores. The photoacoustic signal is directly correlated with the concentration of the endogenous chromophores present in tissue, including melanin, hemoglobin (both oxygenated and deoxygenated), fat, water, and collagen among others (18,19). Hemoglobin dominates the absorption in tissues (except for melanin in the skin) with the highest optical absorption coefficient and therefore has been the focus of most of the studies of endogenous photoacoustic signal. By using multiple wavelengths of laser light (spectroscopic photoacoustic imaging), relative concentrations of specific chromophores can be determined (20–25). A highly applied method, especially in cancer imaging, is to detect the relative amounts of deoxygenated (deoxy) and oxygenated (oxy) hemoglobin (Hb), from which the oxygen saturation ($100\% \times Hb_{oxy}/[Hb_{oxy} + Hb_{deoxy}]$) of the tissue can be calculated (26). This principle is the basis of many clinical trials

where tissue with lower oxygen saturation is considered more likely to be cancerous due to cancer's known hypoxic nature in later stages (27,28).

Beyond using endogenous chromophores, photoacoustic imaging can be used to examine molecular expression of markers that do not naturally absorb light through the use of exogenous contrast agents. When imaging in the "tissue optical window" between 650 and 950 nm where tissue absorption is minimized exogenous agents can be tuned and used to target specific markers or to accumulate passively within tumors due to their poorly structured vasculature (29,30). The main two categories of exogenous contrast agents being explored are plasmonic noble metal nanoparticles and dyes, both of which are noncytotoxic (31,32). Noble metal nanoparticles absorb light strongly due to the enhanced optical absorption caused by strong interactions between electromagnetic waves and the free electron cloud associated with the nanoparticle surface (termed surface plasmon resonance) (33). Furthermore, the optical absorption properties are tunable depending on the synthesized size and shape of the particle, which alters the wavelengths of light at which optimal resonance occurs. However, the clinical use of these particles is limited, and while there are a few clinical trials underway, the Food and Drug Administration (FDA) approval of their use remains elusive. Therefore, clinical research also focuses on the use of already FDA-approved dyes such as indocyanine green and methylene blue (34–38). Due to their small size, these dyes are rapidly cleared from the blood circulation unless conjugated or encapsulated and have lower optical absorption per molecule than do plasmonic nanoparticles. However, the small size also allows for increased tumor penetration and interaction with biomolecules. Besides plasmonic nanoparticles and dyes, many other types of agents have been considered and tested for photoacoustic imaging including carbon nanotubes (39), nanodroplets (40,41), and liposomes and polymer (36) particles. For more

information, please refer to recent reviews (7,31,42,43).

Photoacoustic Imaging Instrumentation

A photoacoustic imaging system typically comprises a pulsed near-infrared laser (532–1100-nm wavelengths, 1–100-nsec pulse width, and 10–50-Hz pulse repetition rate), a US transducer, and a data acquisition and display unit (Fig 2). The laser is often coupled with an optical fiber to deliver light onto the desired region of interest. US transducers can be phased array and positioned on the surface of the region of interest or arranged in photoacoustic CT configuration. Since the data acquisition is common to both photoacoustic and conventional US systems, the integration of the laser into the clinical US scanner is the most economical and efficient means of developing a photoacoustic imaging system, where the same linear or phased array transducer can be used for both US and photoacoustic imaging, thus providing perfectly coregistered images.

Photoacoustic imaging instrumentation can be broadly categorized into preclinical and clinical imaging systems. Preclinical imaging systems typically have a dedicated small-animal positioning platform (with optional heating pad to keep the animal warm during the procedure, heart rate monitoring, and respiratory gating to compensate for motion artifacts) and use high-frequency transducers for high-resolution imaging. These systems are mainly geared toward research and often provide custom image processing software that allows users to perform a multitude of tasks ranging from importing raw data for offline processing, to onboard three-dimensional image reconstruction, and real-time image display. Currently, there are two commercially available preclinical photoacoustic imaging systems as shown in Figure 3: Vevo LAZR (Fujifilm VisualSonics, Toronto, Canada; technology licensed from Seno Medical Instruments, San Antonio, Tex) and Nexus 128 (Endra, Ann Arbor, Mich; technology licensed from OptoSonics, Oriental, NC) (7,44–49). Vevo LAZR uses high-frequency
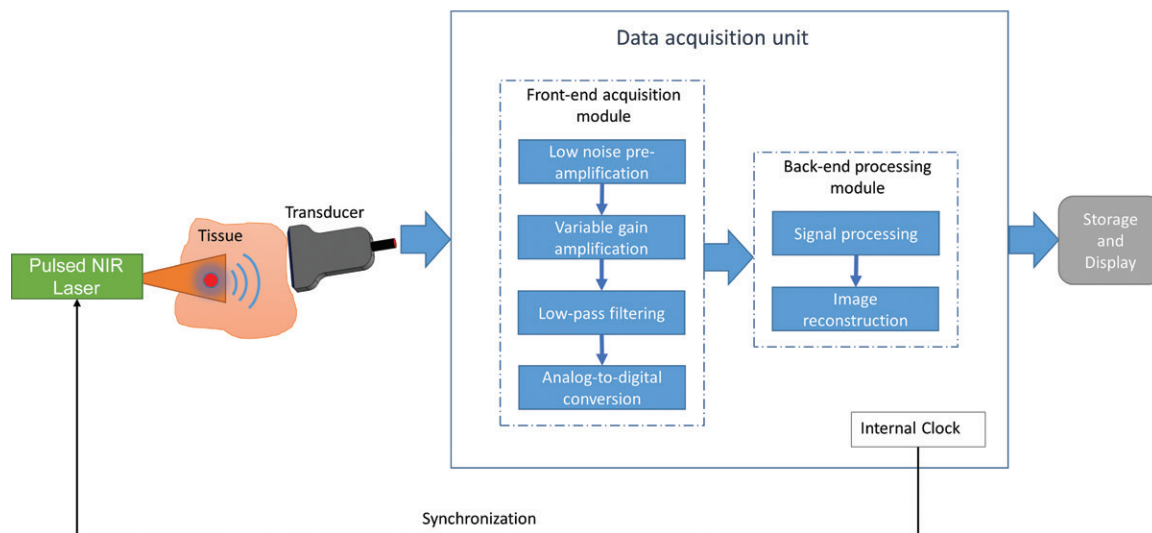
Figure 2

Figure 2: Schematic of photoacoustic imaging instrumentation. When a tissue is exposed to pulsed near-infrared *(NIR)* laser, the pressure transients produced from tissue chromophores are collected by a US transducer scanned over the surface. An internal clock synchronizes the transducer acquisition time to laser firing. The pressure transients are converted by the transducer to time-dependent voltage signals (photoacoustic signals) and are fed into front-end acquisition module where the signals are channeled through a low-noise preamplifier (20–30 dB), followed by a variable gain amplifier (20–50 dB) to achieve a cumulative gain (40–80 dB). The amplified signals are filtered for high-frequency noise components and digitized by using analog-to-digital converters. These digitized signals are further handled by a back-end processing module, which performs a multitude of signal processing and image reconstruction tasks after which the images are appropriately stored and displayed.
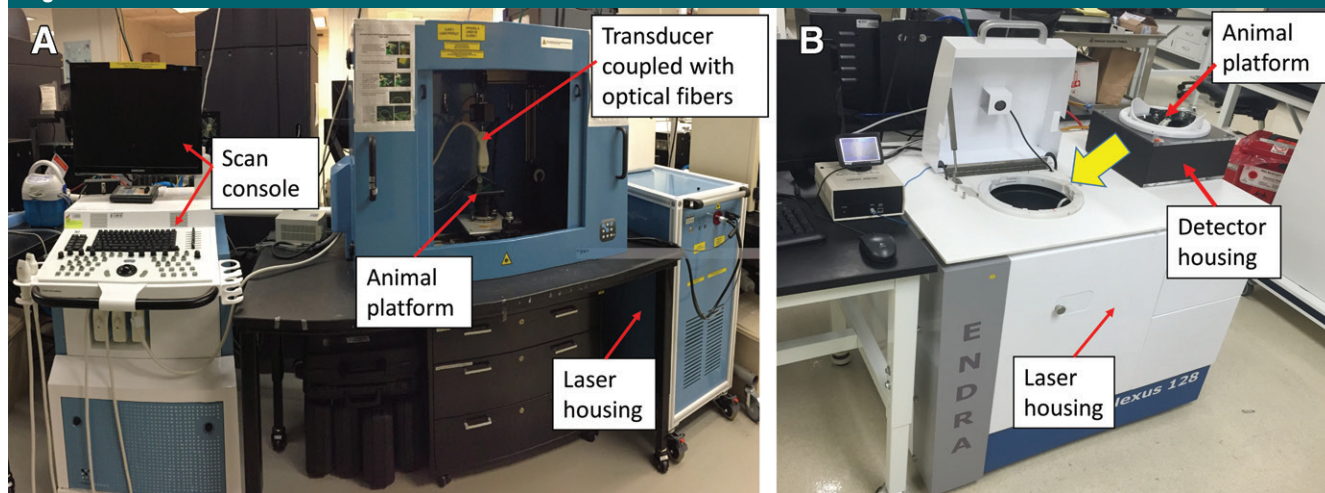
Figure 3

Figure 3: Commercially available preclinical photoacoustic imaging systems. *A,* Vevo LAZR (Fujifilm VisualSonics) uses handheld transducers for laser delivery and photoacoustic signal detection. *B,* Nexus 128 (Endra) uses an animal holder inserted in an aperture consisting of a rotating hemispherical transducer with laser delivered from the bottom. The animal holder is shown outside for illustration purpose.

handheld transducers ranging from 9 to 55 MHz, which limits its use to small-animal imaging, while the Nexus 128 employs a 5-MHz hemispherical transducer array for photoacoustic CT, which is potentially suitable for clinical imaging (however, currently not cleared by FDA for human use).

Clinical photoacoustic imaging systems are a logical extension of preclinical imaging systems and use transducers with clinically relevant frequencies (1–10 MHz). However, unlike preclinical imaging systems where a single transducer configuration may

Ongoing Photoacoustic Imaging Clinical Trials for the Detection of Cancer

Targeted Cancer	Registry	Study	Study Population			Start Date
			No.	Sex	Age (y)	
Breast	ClinicalTrials.gov	LOUIS-3D breast study (124)	96	F	20–70	May 2014
Breast	ClinicalTrials.gov	The PIONEER-01 pivotal study of the Imagio breast imaging system (125)	2000	F	18+	July 2013
Breast	ClinicalTrials.gov	Simulated screening study for breast imaging (126)	160	F	30–80	December 2012
Breast	Netherlands Trial Register	Breast imaging using light and sound (127)	100	F	18+	December 2010
Melanoma–sentinel lymph nodes	German Clinical Trials Register	Photoacoustic tomography in combination with high-resolution US for noninvasive diagnosis of sentinel lymph node in patients with malignant melanoma (128)	120	Both	18+	December 2013
Circulating melanoma cells	ClinicalTrials.gov	In vivo real-time detection of circulating melanoma cells (95)	75	Both	18–80	February 2013
Prostate	ClinicalTrials.gov	Photoacoustic imaging of the prostate: a clinical feasibility study (129)	50	M	18–80	February 2014
Rectum*	ClinicalTrials.gov	Visualization of rectal cancer during endoscopy, using a fluorescent tracer (RAPIDO-TRACT) (130)	30	Both	18+	October 2013

* Photoacoustic endoscopy was optional for patients enrolled in this study.

be sufficient to scan almost any region of interest within the animal, clinical imaging systems are often region specific because different laser-detector configurations are warranted for different applications (eg, tomography is suitable for breast; low-frequency handheld transducer arrays, for internal abdominal organs; high-frequency transducers, for superficial organs such as skin, thyroid; endocavitary arrays, for prostate or ovarian imaging, etc). At the moment, there is no clinical photoacoustic imaging system that is FDA approved and commercially available for human use. Ongoing clinical trials that are currently recruiting patients for cancer imaging (Table) use custom photoacoustic imaging systems, which are still in investigational phase.

Clinical Applications of Photoacoustic Imaging

In the following section, studies that comprise current cancer investigations with clinically translatable photoacoustic imaging systems are presented. A brief summary of photoacoustic imaging instrumentation, imaging protocols, and study details is provided for each clinical application.

Breast Cancer

Breast cancer is the most common cancer among American women and the second leading cause of cancer-related death in women (50). Mammography uses ionizing radiation and has low sensitivity, especially in patients with dense breast tissue. When mammography is combined with other screening techniques such as US or tomosynthesis, the cancer detection rates increase from 6.1/1000 using mammography alone (4.4% false-positive rate) to 8/1000 using mammography plus tomosynthesis (5.3% false-positive rate) and 11.8/1000 using mammography plus US (10.4% false-positive rate) in high-risk women (51,52). When US is used as an adjunctive screening technique to mammography, positive predictive values of as low as 5.6% were reported (53). These rates indicate that many women are called back for unnecessary biopsies, which leads to increased health care costs and psychological stress for women. Therefore, improved breast cancer imaging techniques are needed that can reduce the current false-positive rates while also improving sensitivity (54–56).

Because breast tissue is superficially located and has low optical absorption and US scattering due to its fatty nature, it provides optimal conditions for photoacoustic imaging. The photoacoustic mammoscope developed at the University of Twente (Enschede, the Netherlands) was one of the first systems to perform breast imaging in patients (57). The system consists of an examination table with an aperture to suspend the patient's breast when lying in the prone position (Fig 4). During imaging, the breast is mildly compressed between a glass plate (1064 nm, 10 nsec, 10 Hz, 25 mJ/cm^2) at the cranial side and a planar two-dimensional circular US detector array (80-mm diameter, 590 elements, 1-MHz center frequency) at the caudal side to facilitate three-dimensional imaging. The resolution of this system is 2.3–3.9 mm for depths between 15 and 60 mm, with an average scan time of 30 minutes for a region of interest of 40 × 40 mm^2 comprising of a lesion and normal tissue, as defined by means of x-ray mammography and US. Photoacoustic volumetric images are analyzed for the presence of confined high-signal-intensity regions, and an abnormality is indicated
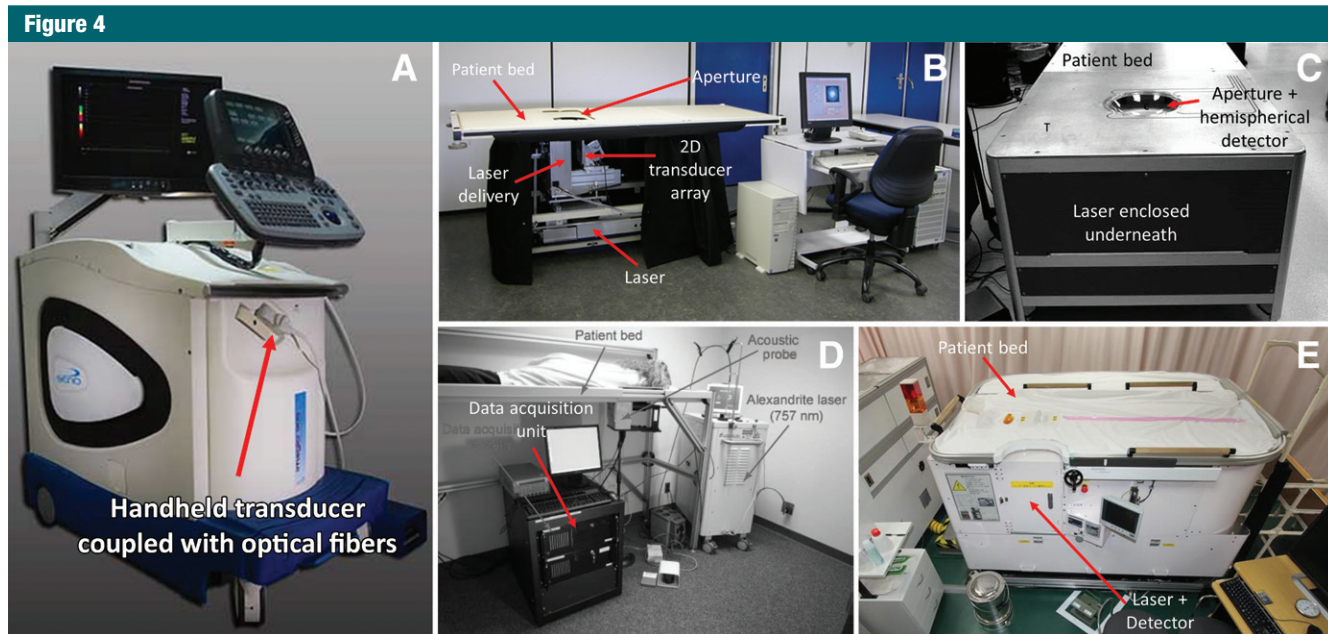
Figure 4

Figure 4: Photoacoustic imaging systems currently used in clinical trials for breast cancer detection. *A,* Imagio (Seno Medical Instruments) uses handheld transducer for breast imaging. Laser is delivered via optical fibers that are attached on either side of the transducer (131). *B,* Photoacoustic mammoscope developed at the University of Twente uses a patient bed with an aperture to insert the breast. Laser is delivered from the cranial side onto the breast, and a planar circular array of US detectors acquires images from the caudal side (132). *2D* = two-dimensional. *C,* Photoacoustic tomography system (Optosonics) consists of a patient bed with an aperture. Laser is delivered from beneath the breast, and a rotating hemispherical array of US transducers acquires photoacoustic images (64). *D,* Laser optoacoustic imaging system (LOIS-64) developed by Ermilov et al consists of a setup similar to the Optosonics system, with a hemispherical array of annular US detectors (60). *E,* Photoacoustic imaging system (Canon) consists of a setup similar to the Twente photoacoustic mammoscope, with laser delivered through both plates and detector coupled to caudal plate (133).

if all the voxels within the region of interest have intensity greater than 50% of the maximum volumetric intensity. Results from an ongoing clinical study that started in 2010 with 17 patients (10 patients suspected of having cancer, two patients with benign cysts, five patients not analyzed) reported an increased contrast (ratio of average intensity value within the abnormal region of interest to average intensity value of the surrounding tissue) in suspected cancer regions compared with the surrounding tissue, with contrast independent of the mammographically estimated breast density (58,59).

Ermilov et al (60) developed a photoacoustic CT system called laser-based optoacoustic imaging system, or LOIS-64, in which the patient lies on an examination table with the breast suspended through an aperture into a hemicylindrical cup with an annular array of detectors (64 elements). The system uses 755-nm laser (70-mm

circular beam, 10 Hz, 10 mJ/cm²) and custom data acquisition system (Fig 4). A preliminary clinical study imaged mammographically suspected breast lesions in 27 patients with US and photoacoustic imaging. If an isolated area corresponding to a US or mammographically suspected lesion had increased photoacoustic intensity, it was considered a tumor. Biopsy revealed 26 malignant and eight benign lesions. The LOIS-64 identified correctly 18 of 26 malignant lesions and four of eight benign lesions (60). In 2010, the authors introduced a combined photoacoustic and ultrasonic imaging system (called Imagio; Seno Medical Instruments, San Antonio, Tex) utilizing a two-laser system (1064 nm and 755 nm) and a handheld commercial linear US array (128 elements, 5 MHz) for real-time data acquisition (61). The Imagio system (received CE Mark approval in Europe) is currently being used as an investigational device in a

large, multicenter prospective clinical trial in the United States with an estimated enrollment of 2000 patients (Fig 4). Preliminary results (Fig 5) from 66 patients (37 cancers and 29 benign lesions proven histologically) showed a sensitivity and specificity of 100% and 72%–79%, respectively (62,63).

Kruger et al (64) modified the Nexus 128 preclinical photoacoustic CT system (OptoSonics, Oriental, NC), which is licensed to Endra (Ann Arbor, Mich), for clinical use. The system uses a setup similar to that of LOIS-64 using an examination table with circular aperture consisting of a hemispherical array of spirally arranged US detectors (512 circular elements, 2 MHz) and an FDA-approved 756-nm laser (Fig 4). Photoacoustic CT was performed in four healthy patients and demonstrated the feasibility of clinical breast imaging with submillimeter resolution (64). The scanning time was reported to be between 12 seconds and 3.2 minutes for
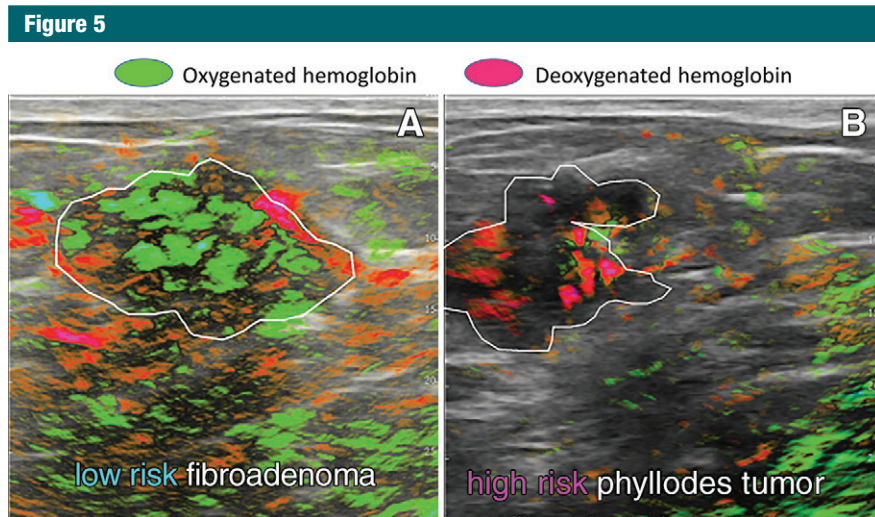
Figure 5

Figure 5: Clinical photoacoustic images overlaid on US images show endogenous photoacoustic signals corresponding to oxygenated and deoxygenated hemoglobin in breast lesions. *A,* Solid lesion with high oxygenated hemoglobin concentration. Lesion was confirmed at biopsy as benign fibroadenoma. *B,* Solid lesion with high deoxygenated hemoglobin concentration. Lesion was confirmed at biopsy as phyllodes tumor. (Reprinted, with permission, from reference 63.)

spiral sizes ranging from 24-mm to 96-mm radius, with a spatial resolution of 0.42 mm.

Another group, Kitai et al (65), used a photoacoustic imaging system (Canon, Tokyo, Japan; technology licensed from OptoSonics, Oriental, NC), in which the patient lies in a prone position on a table with the breast suspended through a rectangular aperture (17 cm × 18 cm) and mildly compressed between two plates craniocaudally beneath the table (Fig 4). Laser light is delivered onto the breast through both plates while the detector is coupled to the caudal plate. The system uses a dual-illumination laser delivery scheme (756 nm, 797 nm, 825 nm, and 1064 nm) and a rectangular two-dimensional US array (15 × 23 elements, 1 MHz) to acquire 30 mm × 46 mm scans in 45 seconds. Photoacoustic imaging, conventional mammography, magnetic resonance (MR) imaging, and US were performed in 26 biopsy-confirmed breast cancer patients enrolled in a preliminary clinical trial. All patients underwent breast surgeries within 1 month of photoacoustic imaging, and the excised specimens were pathologically examined.

Preoperative diagnosis concluded that 26 patients had 27 lesions, of which 21 were invasive breast cancers, five were ductal carcinoma in situ, and one was a phyllodes tumor. Tumors were considered visible with the photoacoustic imaging system if the photoacoustic signal was located at the site of known tumor from the correlated MR images. It was reported that 15 of 21 invasive breast cancers, five of five ductal carcinomas in situ, and zero of one phyllodes tumor were visible, corresponding to 74% (20 of 27) tumor visibility. On the basis of photoacoustic images acquired at 757 nm and 797 nm, mean oxygen saturation of hemoglobin and mean total hemoglobin concentration were calculated and estimated as 78.6% (53.7%–100%) and 207 μM (87–309 μM), respectively.

Management and staging of breast cancer is another potential clinical application besides detection and characterization of the primary breast tumor. Sentinel lymph node biopsy is used to help stage breast cancer. The sentinel lymph node is an individual or a group of nodes into which the primary tumor first drains in the regional lymphatic basin and thus is the most likely (usually axillary) node

to harbor metastatic breast cancer (66). Sentinel lymph node biopsy is a surgical procedure in which a radioactive colloid (technetium sulfur) followed by blue dye (isosulfan blue or methylene blue) are injected intradermally around the tumor periphery (67). Within a few minutes after the blue dye injection, the axillary region is surveyed by using a handheld Geiger counter, and a surgical incision is made upon radioactivity confirmation. Nodes that have been stained blue or show increased radioactivity are removed for histologic confirmation of possible metastasis. Since photoacoustic imaging is well suited for detecting chromophore (blue dye), it holds potential to complement the sentinel lymph node biopsy technique and avoid the use of radioactive colloid altogether. Erpelding and colleagues (68–70) developed a photoacoustic imaging system (laser: 667 nm, 6.5 nsec, 10 Hz, 10 mJ/cm^2; detector–handheld linear array with nominal bandwidth of 4–8 MHz and imaging frame rate of 5 Hz) by modifying a clinical US scanner (iU22; Phillips Health Care, Andover, Mass) and reported its use on patients (70) to noninvasively detect sentinel lymph nodes. Their goal was to accurately identify sentinel lymph nodes by using photoacoustic imaging and perform minimally invasive fine-needle aspiration biopsy to sample sentinel lymph nodes instead of performing surgery. Methylene blue (5 mL, 2 mg/mL) was injected subcutaneously with a 25-gauge needle near the areola in the same breast quadrant as the primary tumor and allowed to drain for 5 minutes. Photoacoustic imaging was then performed to identify sentinel lymph nodes based on the optical absorption of methylene blue. Results from one patient were reported, which indicate that the sentinel lymph node was visualized on coregistered photoacoustic and US images indicating possible metastasis. Further results are awaited for this trial to assess whether this technique actually allows consistent sentinel lymph node detection with successful image-guided fine-needle aspiration of positive nodes to potentially avoid surgery.

In a further attempt to image metastatic sentinel lymph nodes noninvasively

as an alternative to sentinel lymph node biopsy, Luke et al (71) developed molecularly activated plasmonic nanosensors (40-nm gold nanoparticles targeted to a cancer biomarker called epidermal growth factor receptor [72–74]) and performed spectroscopic photoacoustic imaging (680–860 nm, 20-nm increments) with a 40-MHz linear array (Vevo LAZR; Fujifilm VisualSonics) on an orthotopic nude mouse model of squamous cell carcinoma of the oral cavity. Molecularly activated plasmonic nanosensors were injected peritumorally after which coregistered US and photoacoustic images were acquired continuously for 2 hours, over a three-dimensional volume encompassing lymph nodes. Spectroscopic analysis was performed to differentiate photoacoustic signals of molecularly activated plasmonic nanosensors from deoxyhemoglobin and oxyhemoglobin. Results indicate that a strong increase in the photoacoustic signal was observed in sentinel lymph nodes harboring metastases within 2 hours of molecularly activated plasmonic nanosensors injection. A sensitivity of 100% and a specificity of 87.5% were reported, with detection ability of metastases as small as 50 μm.

Prostate Cancer

Prostate cancer is the second leading cause of cancer death in American men (50). Currently, screening is performed by using prostate-specific antigen blood test and digital rectal examination, which has high rates of false-positives and false-negative findings. Transrectal US-guided biopsy has limited sensitivity and is reported to miss cancer in more than 30% of the patients (75). Photoacoustic imaging combined with transrectal US may be able to provide anatomic, functional, and molecular information of prostate cancer, potentially improving the yield of US-guided biopsy, and may be helpful for prognostication of patients with prostate cancer on active surveillance.

Several research groups have conducted photoacoustic imaging of prostate cancer in vivo using animal models (76–80). Levi et al (81,82) developed a photoacoustic contrast agent labeled AA3G-740 that binds to gastrin-releasing peptide receptor, which is reported to be highly overexpressed in prostate cancer. In vivo molecular photoacoustic imaging of mice ($n = 6$) bearing PC3 human prostate cancer cells was performed 30 and 60 minutes after contrast agent injection by using the Nexus 128 photoacoustic CT system (Endra). AA3G-740 was able to bind to gastrin-releasing peptide receptor in mice even in poorly vascularized tumors, leading to nearly twofold increase in the photoacoustic signal relative to a control contrast agent (82). It was also reported that the smallest number of AA3G-740–labeled PC3 cells required to produce background differentiable photoacoustic signal was only 0.5 million (1-cm^3 tumor may have up to 100 million cells), which demonstrates the potential of molecular photoacoustic imaging to detect prostate cancer at small sizes.

In an ex vivo study (83), 42 prostate specimens (grossly sectioned from 30 prostate glands) from 30 patients with biopsy-confirmed prostate cancer were imaged within 1 hour of prostate resection by using a custom photoacoustic imaging system (84). The system uses a tunable pulsed laser (700–1000 nm) and a linear US array (32 elements, 5 MHz) coupled with an acoustic lens to achieve real-time focusing, along with dual-axis stepper motors for three-dimensional data acquisition with a scan time of 5 minutes for 45 mm × 45 mm. Histopathologic evaluation confirmed 16 of 42 specimens as malignant, eight of 42 as benign prostatic hyperplasia, and 18 of 42 as normal. Photoacoustic images of normal, benign prostatic hyperplasia, and malignant specimens were decomposed into spectroscopic images representing deoxyhemoglobin, oxyhemoglobin, lipid, and water. Histopathologic images marked with normal, benign prostatic hyperplasia, and malignant lesions were coregistered with spectroscopic photoacoustic C-scan (coronal plane) images, and mean photoacoustic signal intensities of regions of interest corresponding to each pathologic condition were compared. Results indicate that there was a statistically significant difference in mean photoacoustic signal intensity of

deoxyhemoglobin ($P < .0001$) and lipid ($P = .0251$) between malignant and normal prostate. A significant difference in mean intensity of deoxyhemoglobin ($P < .0001$) was reported between malignant prostate and benign prostatic hyperplasia. No statistically significant difference was reported between benign prostatic hyperplasia and normal prostate for deoxyhemoglobin, oxyhemoglobin, lipid, and water. A higher mean photoacoustic intensity indicating stronger absorption of deoxyhemoglobin ($P < .0001$) was reported for malignant tissue compared with nonmalignant (benign plus normal) prostate tissue, with a sensitivity of 81.3% and specificity of 96.2% (83).

Photoacoustic imaging has also been explored for monitoring treatment delivery for prostate cancer. Brachytherapy is one of the treatment approaches for prostate cancer in which multiple tiny seeds filled with radioactive substances are implanted in the cancerous region within the prostate (85). Real-time seed localization, which is a crucial step in guiding and implanting the brachytherapy seeds in prostate, is currently performed by using transrectal US (86). Since the seeds are small, often they cannot be visualized at US. Currently, the seed location is confirmed either by using postprocedural x-ray CT or MR imaging. More sensitive techniques are desired to visualize real-time seed deployment. Bell et al (87) have conducted an in vivo study in which three brachytherapy seeds (4.5 mm long and 0.8 mm diameter) coated with black ink were inserted into a dog's prostate. A 1064-nm laser beam was delivered onto the prostate via an optical fiber transperineally, and the combined photoacoustic and US images were detected (Fig 6) by using a 7-MHz linear (BPL9–5/55; Ultrasonix, Richmond, Canada) and 6-MHz curvilinear (BPC8–4/10; Ultrasonix) transrectal US probes. Results indicate that the brachytherapy seeds were visualized within the laser maximum permissible exposure limits.

Skin Cancer

Another active research area for photoacoustic imaging is the detection and
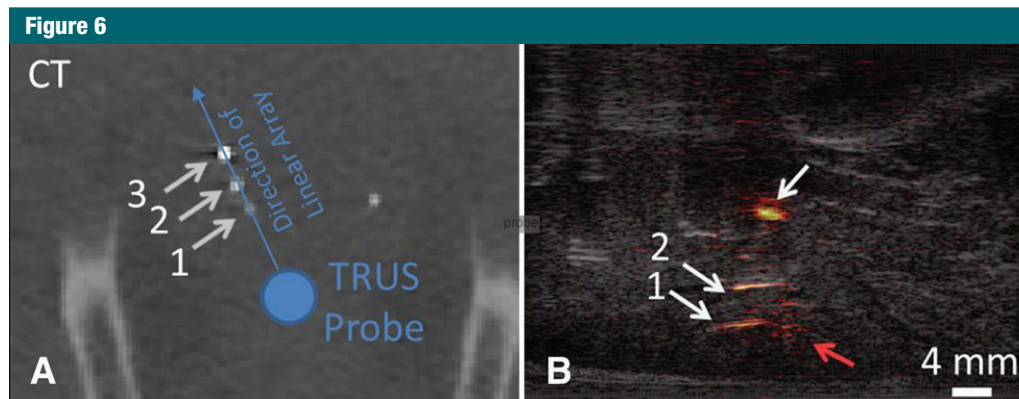
Figure 6: Visualization of coated brachytherapy seeds in canine prostate in vivo. *A,* Postoperative CT scan shows location of seeds (arrows) with respect to the intraoperative transrectal US *(TRUS)* probe. *B,* Combined photoacoustic and gray-scale US image. Two of the three implanted brachytherapy seeds were visualized on the photoacoustic image. Red arrow = photoacoustic response from the location of the fiber, white unlabeled arrow = signal of unknown origin. (Adapted and reprinted, with permission, from reference 87.)

local staging of skin cancer. Melanoma (< 5% of skin cancers) is the most aggressive type of skin cancer and is associated with approximately 75% of skin cancer-related deaths (88). Early detection of melanoma followed by surgical resection is the best means of reducing mortality from this deadly disease. Currently, melanoma is screened by performing a whole-body skin examination. Following the physical examination, if any lesion is suspected because of changes in color, texture, shape or size, the physician assesses it more closely using a dermoscope (89). Biopsy is performed on suspected moles followed by histopathologic analysis for diagnosis. Since the selection of suspicious moles for biopsy is rather subjective to the physician's decision (90), there is a risk of missing cancerous moles and unnecessary excision of benign moles. In its latest report, the U.S. Preventive Services Task Force has concluded that there is insufficient evidence to recommend for or against screening for skin cancer by using whole-body skin examination by a physician or patient (91). Since most melanomas contain melanin and undergo physiologic changes, photoacoustic imaging with its ability to quantify the distribution of melanin, size of mole, and shape of mole may aid in differentiation of melanoma from other benign moles that contain melanin.

Photoacoustic imaging of melanoma has been investigated in several animal models (92–96). For instance, Wang et al (97) developed a handheld photoacoustic microscopy system (650-nm laser, 25-MHz focused single-element US transducer) for melanoma detection and conducted in vivo experiments on subcutaneous melanoma mouse tumor models. To image the entire tumor depth, the system uses annular laser beam delivery via optical fibers arranged in a circle around the US transducer. Both the transducer and optical fiber arrangement were linearly scanned inside a stationary handheld probe housing motorized linear translation stage to acquire tumor images. To perform a 10-mm linear scan, the acquisition time was reported as 10 seconds. A 3.66-mm-thick melanoma with clearly visible top and bottom tumor boundaries was visible on the images. This was in close agreement with measurement (3.75 mm) performed after melanoma excision.

The presence of metastasis in lymph nodes is one of the most important factors in staging of melanoma. In a study to detect possible melanoma metastases, Langhout and colleagues have investigated photoacoustic imaging of sentinel lymph nodes in patients with cutaneous melanoma (96,98). Spectroscopic photoacoustic imaging (700 nm, 732 nm, 757 nm, 800 nm, and

820 nm at 20 Hz and 15 mJ/cm^2) was performed in 0.2-mm increments on three metastatic and nine benign lymph nodes excised from eight melanoma patients undergoing lymphadenectomy by using a 21-MHz linear US array (Vevo LAZR, Fujifilm VisualSonics) at 20-minute scans for each node (98). Results indicate that metastasized melanin was differentially detected from blood in resected human lymph nodes. A similar study of resected lymph nodes excised from patients with cutaneous melanoma who underwent lymphadenectomy was conducted by Jose et al (96). A custom-built spectroscopic photoacoustic imaging system (720 nm, 760 nm, 800 nm, 850 nm, at 10 Hz and 12 mJ/cm^2) with top-down illumination and a curvilinear US detector array (6.25 MHz, 32 elements) rotated around the sample requiring 4 minutes per wavelength to acquire 18 projections of each lymph node was used in the study. Results from only one patient were reported so far indicating that their system was able to detect strong photoacoustic signal intensity throughout the lymph node (at 5 mm depth from the surface), which was diagnosed later as melanoma through histopathologic evaluation.

In another study, Favazza et al (99) investigated photoacoustic imaging to characterize melanocytic nevus (mole), a common benign skin lesion that can have similar characteristics
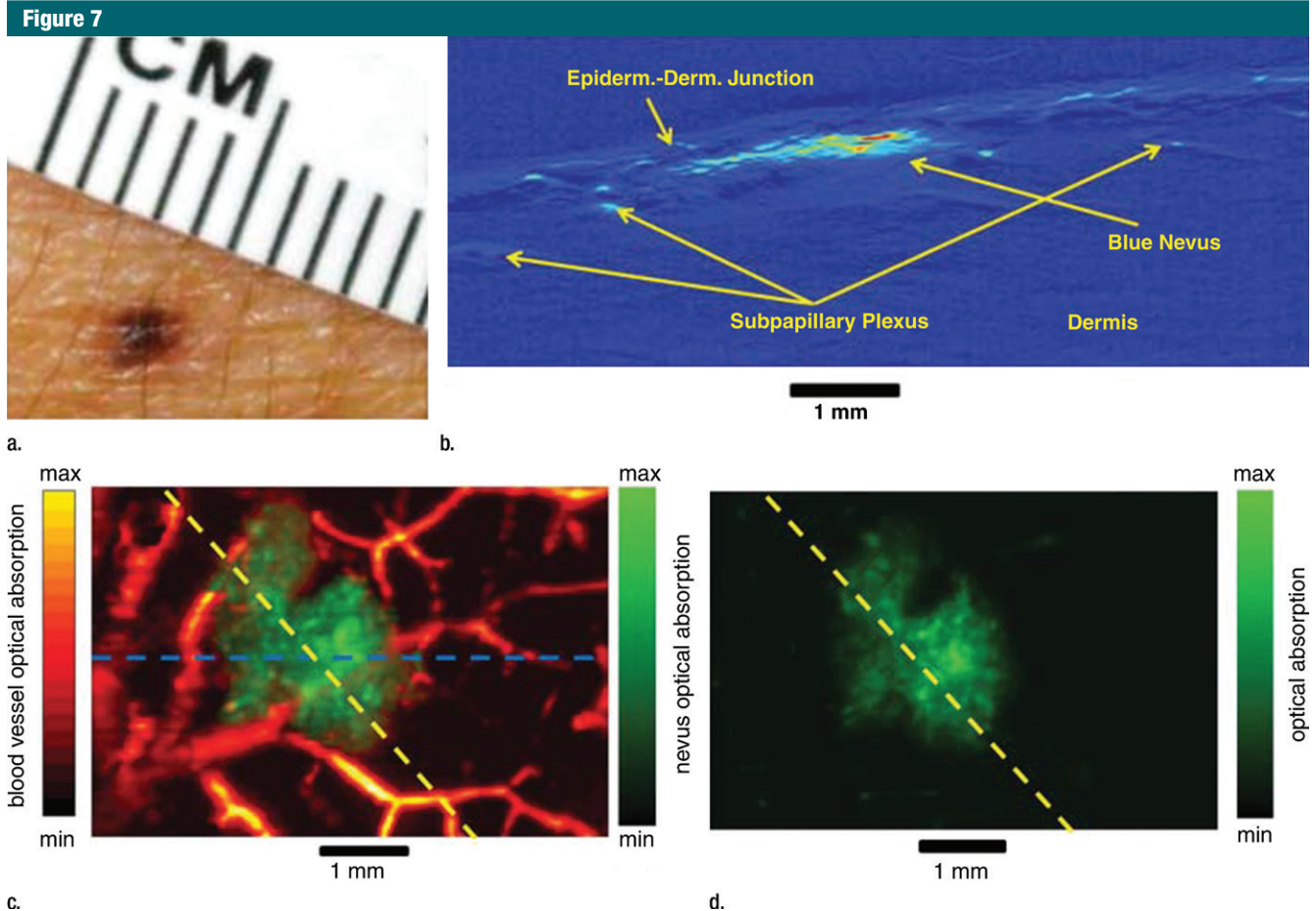
Figure 7

Figure 7: *A,* Photograph of a melanocytic nevus located on the forearm of a healthy volunteer. *B,* Photoacoustic B-mode image taken along the blue dashed line in, *C.* Notable features include the nevus, epidermal–dermal junction, and subpapillary blood vessels (all labeled). *C,* Maximum amplitude projected photoacoustic image of the nevus acquired at 570-nm wavelength. The nevus is clearly shown in green scale, and blood vessels are shown in red. *D,* Photoacoustic image acquired at 700-nm laser excitation wavelength shows nevus only without any blood vessels. (Adapted and reprinted, with permission, from reference 99.)

of melanoma and thus can be difficult to differentiate. Photoacoustic microscopy imaging was performed using a custom system employing a dye laser (570 nm, and 700 nm, 500 Hz) and a 50-MHz single-element US transducer (V214-BB-RM; Panametrics, Waltham, Mass) connected to a motorized translation stage. The system was scanned for 5–10 minutes on the forearm of a human volunteer (Fig 7) at 20-µm increments in horizontal and vertical directions to acquire a three-dimensional volumetric image of a 6 mm × 4 mm area with nevus. Results indicate that they were able to differentiate nevus from the surrounding blood vessels. From the photoacoustic images, the dimensions of nevus were measured

as 262–270-µm thick, 2.64–2.66-mm wide, and located 135–140-µm deep below the skin surface. When measured histologically, the nevus was 450-µm thick, 2.18-mm wide, and located 150 µm deep below the surface, with measurement variations attributed to excised tissue handling. Although these results establish the potential of photoacoustic imaging in melanoma detection in general, a more detailed study investigating whether melanoma can be differentiated from benign nevi containing melanin has not yet been reported.

Thyroid Cancer

Photoacoustic imaging may also be valuable in the characterization of thyroid nodules. Benign thyroid nodules

are common with a 5% or lower malignancy rate and are routinely detected by using US in 40%–50% of the population (100–102). Although standard B-mode US can characterize many thyroid lesions as definitively benign based on imaging patterns (103), nodules without definitive benign features or nodules of certain size still require US-guided fine-needle aspiration biopsy. However, biopsy is invasive, expensive, impractical (when multiple nodules are present), and indeterminate in up 25% of patients depending on the technique (104). Moreover, biopsy results are sometimes inconclusive, especially if the lesion has follicular growth pattern, such as follicular adenoma or follicular carcinoma (105), requiring surgery to
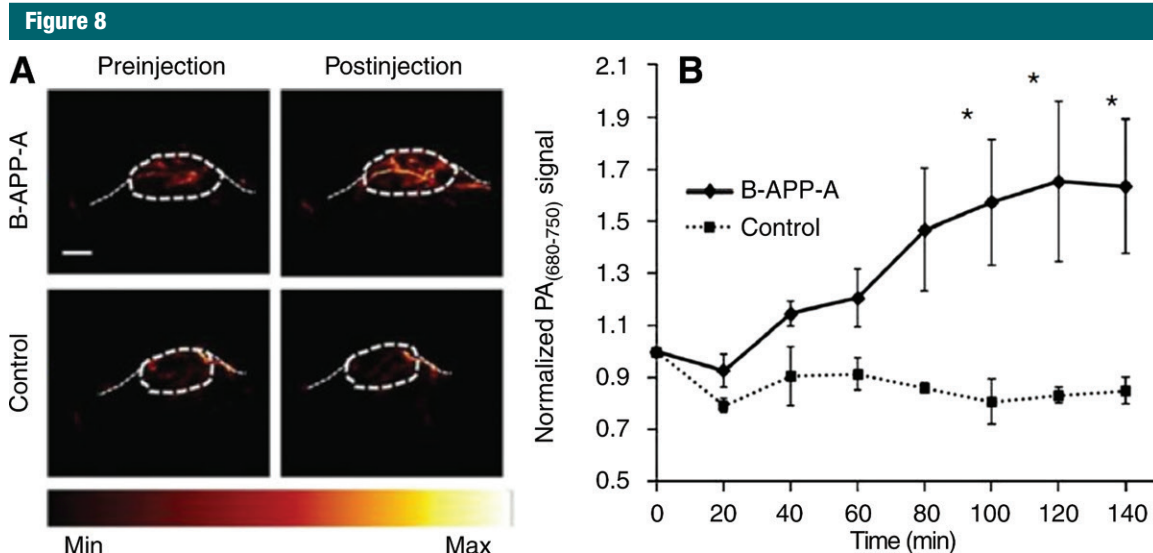
Figure 8: Molecular photoacoustic imaging of thyroid cancer using a photoacoustic contrast agent B-APP-A that specifically binds to follicular thyroid cancer biomarkers MMP-2 and MMP-9. Mice bearing follicular thyroid cancers in the hind legs underwent photoacoustic imaging at 680 and 750 nm before and after intravenous injection of 4.8 nmol of the activatable probe B-APP-A and a noncleavable control probe. *A*, The subtraction photoacoustic signal at 140 minutes after injection was approximately 1.7-fold higher than the preinjection signal for the active probe. The subtraction signal for the control probe did not change over time. At early time points, the difference in subtraction signal was not significantly different for the two probes. Over time, the signal for the activatable probe steadily increased, becoming significantly different at 100 minutes. *MMP* = matrix metalloproteinase, *B-APP-A* = Alexa750-CXeeeeXPLGLAGrrrrrXK-BHQ3. *B*, Graph shows that subtraction photoacoustic *(PA)* signal was normalized by the preinjection subtraction photoacoustic signal: $(PA_{680\ nm} - PA_{750\ nm})$ after injection/$(PA_{680\ nm} - PA_{750\ nm})$ before injection. Error bars = standard error ($n = 5$ for B-APP-A, $n = 4$ for control probe). ∗ = $P < .05$. Scale bar = 0.25 cm. (Reprinted, with permission, from reference 106.)

confirm malignancy. Therefore, diagnostic approaches that can either rule in benignity or confirm malignancy accurately and noninvasively are warranted, avoiding biopsies and unnecessary surgeries.

In a preclinical study by Levi and colleagues (106) that evaluated molecular photoacoustic imaging of thyroid cancer, the presence of two specific follicular thyroid cancer biomarkers matrix metalloproteinase MMP-2 and MMP-9, which can be targeted by using a MMP-activatable photoacoustic probe, Alexa750-CXeeeeXPLGLAGrrrrrXK-BHQ3, or B-APP-A, was reported. In vivo photoacoustic imaging was performed on nude mice bearing follicular carcinoma tumors at 680 and 750 nm prior to and after intratumoral injection by using the Vevo LAZR system ($n = 3$ for 0.6-nmol B-APP-A and $n = 3$ for 0.6-nmol noncleavable control probe) and after intravenous injection by using the Nexus 128 photoacoustic CT system ($n = 5$ for 4.8-nmol B-APP-A and $n = 4$ for

4.8-nmol noncleavable control probe). Cleaving enables the activatable probes to provide signal only after activation by a target, which results in higher detection sensitivity and specificity compared with those with conventional probes that provide signal regardless of their proximity or interaction with target tissue (107). Photoacoustic signal corresponding to the cleavage of B-APP-A probe was obtained by subtracting signal acquired at 750 nm from signal acquired at 680 nm. Photoacoustic signal intensities from the control probe at both wavelengths were found to be similar, making the control probe photoacoustically silent on subtraction (Fig 8). Tumors injected with B-APP-A showed significantly higher normalized subtraction photoacoustic signal than did tumors injected with noncleavable control probe, suggesting that the diagnosis of follicular carcinoma could be made on the basis of noninvasive visualization of the presence of cancer-specific biomarkers.

Dogra et al (108) have conducted an ex vivo study to detect thyroid cancers in patients using photoacoustic imaging. Their system used a fiber-coupled tunable laser (700–1000 nm), a linear US array (32 elements, 5 MHz), and a spherical acoustic lens housed together in a probe that is connected to a dual-axis translation stage. Spectroscopic photoacoustic imaging (760 nm, 850 nm, 930 nm, and 970 nm) was performed immediately following resection of 88 thyroid lesions (13 malignant and 75 benign) harvested from 50 patients who underwent total or partial thyroidectomy. Laser light was delivered onto each thyroid specimen placed in a sample holder, from the bottom, and the probe was raster scanned on top of the specimen to acquire a three-dimensional data set. Histopathologic examination of each imaged thyroid section was performed, and areas that included normal, benign, and malignant thyroid tissue were marked on the slides. Digital images of labeled slides
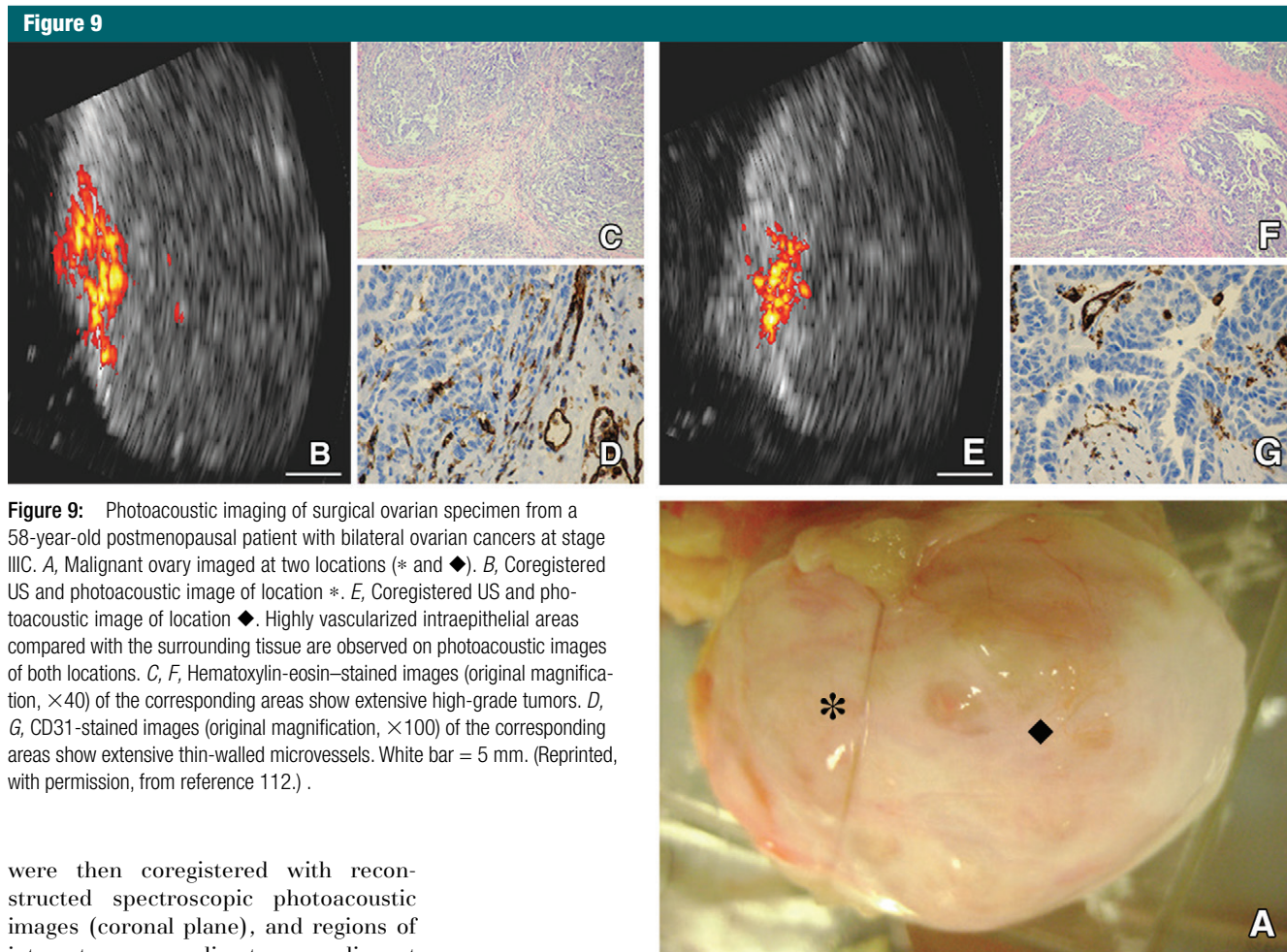
Figure 9

Figure 9: Photoacoustic imaging of surgical ovarian specimen from a 58-year-old postmenopausal patient with bilateral ovarian cancers at stage IIIC. *A,* Malignant ovary imaged at two locations (∗ and ◆). *B,* Coregistered US and photoacoustic image of location ∗. *E,* Coregistered US and photoacoustic image of location ◆. Highly vascularized intraepithelial areas compared with the surrounding tissue are observed on photoacoustic images of both locations. *C, F,* Hematoxylin-eosin–stained images (original magnification, ×40) of the corresponding areas show extensive high-grade tumors. *D, G,* CD31-stained images (original magnification, ×100) of the corresponding areas show extensive thin-walled microvessels. White bar = 5 mm. (Reprinted, with permission, from reference 112.) .

were then coregistered with reconstructed spectroscopic photoacoustic images (coronal plane), and regions of interest corresponding to nonmalignant and malignant tissue were drawn on the photoacoustic images. Mean photoacoustic signal intensity of each region of interest was then computed for spectrally resolved deoxyhemoglobin and oxyhemoglobin images. An increase in mean photoacoustic signal intensity of deoxyhemoglobin was reported in malignant tissue compared with benign tissue. The sensitivity and specificity in differentiating malignant from nonmalignant thyroid tissue ex vivo were 69.2% and 96.9% respectively.

Ovarian Cancer

Among gynecologic malignancies, ovarian cancer has the highest mortality rate, accounting for 5% of cancer deaths among women (109). Since ovarian cancer is relatively uncommon, current screening techniques that involve general population for detection

of ovarian cancer are ineffective, with poor sensitivity and specificity (110). A large randomized multicenter clinical trial (111) performed in the United States to determine the effect of screening on ovarian cancer mortality concluded that simultaneous screening with CA-125 (serum biomarker for ovarian cancer) and transvaginal US did not reduce ovarian cancer mortality when compared with usual care. Therefore, techniques that can aid in earlier and more accurate detection of ovarian cancer are warranted. Photoacoustic molecular imaging may be a suitable candidate to complement existing screening techniques including transvaginal US for improved detection and characterization of ovarian cancer.

Aguirre et al (112) have reported the development of a coregistered photoacoustic and US imaging system suitable for ex vivo imaging of ovaries. The system uses a tunable laser (740 nm, 12 nsec, 15 Hz) and a custom-developed 1.75-dimensional transducer array (5 MHz). With this system, an ex vivo study was performed on 33 human ovaries extracted from patients who underwent oophorectomy. The system was able to differentiate normal postmenopausal versus malignant postmenopausal ($P = .0237$) ovaries, with sensitivity and specificity of 83% and 83%, respectively, while no significant differences were found between normal premenopausal versus normal postmenopausal ($P = .2361$) ovaries (Fig 9). The group (113,114) later reported

Radiology

an upgraded system built specifically for clinical use that employs a laser (750 nm, 20 ns, 15 Hz) and modified a commercial transvaginal US probe (6 MHz) by mounting an array of 36 optical fibers around the probe to facilitate in vivo photoacoustic imaging. Fresh excised ovaries from a 40-year-old premenopausal patient with ovarian cancer were imaged with the upgraded system to demonstrate the potential of their system for in vivo diagnosis of ovarian cancer.

Cervical Cancer

Cervical cancer is another interesting application for photoacoustic imaging. Diagnosis of cervical cancer often starts with an abnormal pap screening results followed by colposcopy and biopsy for confirmation. Peng et al (115) have conducted an in vitro study for photoacoustic imaging of cervical cancer for the first time. Photoacoustic imaging was performed on frozen biopsy samples (3–6 mm in size) harvested from 30 patients who underwent cervical colposcopical screening. Each frozen sample was divided into two pieces, one for photoacoustic imaging and the other for histopathologic evaluation. In each imaging session, one piece of normal tissue and one piece of the lesion from the same patient were embedded on a cylindrical agar phantom (separated 1–2 mm apart at a depth of 5 mm from surface), simulating optical properties of a human cervix, and scanned with a custom photoacoustic imaging system (fiber coupled 532-nm laser with spot size 1 mm, 10-MHz focused transducer). Staging was performed on the basis of the clinical results of each patient obtained from colposcopy and histologic examination, confirming one of 30 samples as cervical intraepithelial neoplasia (CIN) 2, six of 30 as CIN 3, 12 of 30 as cervical cancer (CC) 1, 10 of 30 as CC 2, and one of 30 as CC 3. Results showed increased mean signal intensity representing increased mean optical absorption of cervical lesions compared with normal cervical tissue samples. A high correlation of 0.9431 between staging of cervical cancer and the mean optical

absorption was reported, implying that the mean optical absorption increases almost monotonically with the severity of cervical cancer.

Challenges and Future Outlook

Besides the advantages of photoacoustic imaging (high optical contrast, high spatial resolution, cost-effectiveness, real-time imaging), several challenges need to be overcome. Radiologists are likely to be the early adopters of photoacoustic imaging, requiring training with laser and interpretation of the new information and images obtained from photoacoustic imaging. At the moment, there is a wide range of in-house systems available for photoacoustic imaging for the same application that varies greatly in terms of the laser, transducers, image acquisition ability, and display capabilities. With most of the photoacoustic imaging systems still in prototype phase, it is difficult to compare results from different systems even if similar testing conditions were used. For example, image metrics corresponding to the same lesion acquired by one system might be different from those acquired with other systems due to factors such as operator dependency, laser fluence, and image acquisition settings. Therefore, a standardized clinical system needs to be developed and able to be purchased by a wide array of scientists and clinicians to increase the development and standardization of current clinical applications if a true transition to clinic is to be expected.

Furthermore, several adaptations to prototype systems need to be undertaken to leverage the cost advantage and portability of US, which is the primary drive for its widespread adoption. For example, there is a need for the development of small, low-cost, pulsed lasers with high repetition rates that can integrate into the existing US scanners and enable real-time photoacoustic imaging in a clinical setting. Moreover, clinically translatable contrast agents will need to be developed and suitable cancer biomarkers need to be identified to aid in photoacoustic molecular imaging beyond endogenous chromophores.

Conclusion

Photoacoustic imaging, which is complementary to US imaging, has been extensively examined in preclinical studies during the past decade. Currently, there is a broad effort to expand photoacoustic imaging to clinical applications for cancer imaging. In this review, basics and general principles of photoacoustic imaging along with cancer-specific applications of photoacoustic imaging that can be readily translated to clinic were discussed. With the availability of commercial preclinical imaging systems along with the ability to build relatively inexpensive custom systems, an increase in photoacoustic imaging investigation rate is expected in the coming years for various clinical applications, including and beyond cancer detection and characterization (47,116–123).

References

1. Wang LV, Hu S. Photoacoustic tomography: in vivo imaging from organelles to organs. Science 2012;335(6075):1458–1462.

2. Manohar S, van Apeldoorn A, Taruttis WS. Photoacoustic imaging: cells make themselves heard. Nat Photonics 2015;9:216–218.

3. Bell AG. Production of sound by radiant energy. Science 1881;2(49):242–253.

4. Wang LV, Wu HI. Biomedical optics, principles and imaging. J Biomed Opt 2008; 13(4):049902.

5. Oraevsky AA, Karabutov AA. Optoacoustic tomography. In: Vo-Dinh T, ed. Biomedical photonics handbook. Boca Raton, Fla: CRC, 2003.

6. Emelianov SY, Aglyamov SR, Karpiouk AB, et al. Synergy and applications of ultrasound, elasticity, and photoacoustic imaging. Proc IEEE Ultrason Symp 2006; 405–415.

7. Wilson KE, Wang TY, Willmann JK. Acoustic and photoacoustic molecular imaging of cancer. J Nucl Med 2013;54(11):1851–1854.

8. Chen YS, Frey W, Kim S, Kruizinga P, Homan K, Emelianov S. Silica-coated gold nanorods as photoacoustic signal nanoamplifiers. Nano Lett 2011;11(2):348–354.

9. Weissleder R. A clearer vision for in vivo imaging. Nat Biotechnol 2001;19(4):316–317.

10. Frangioni JV. In vivo near-infrared fluorescence imaging. Curr Opin Chem Biol 2003;7(5):626–634.

11. Allen TJ, Beard PC. Dual wavelength laser diode excitation source for 2D photoacoustic imaging. In: Oraevsky AA, Wang LV, eds. Proceedings of SPIE: medical imaging 2007—photons plus ultrasound: imaging and sensing 2007: The Eighth Conference on Biomedical Thermoacoustics, Optoacoustics, and Acousto-optics. Vol 6437. Bellingham, Wash: International Society for Optics and Photonics, 2007; 64371U.

12. Laser Institute of America. American National Standard for Safe Use of Lasers: ANSI Z136.1-2000. New York, NY: Laser Institute of America, 2007.

13. Chan V, Perlas A. Basics of ultrasound imaging. In: Narouze S, ed. Atlas of ultrasound-guided procedures in interventional pain management. New York, NY: Springer, 2011; 13–19.

14. Wang LV. Tutorial on photoacoustic microscopy and computed tomography. IEEE J Sel Top Quantum Electron 2008;14(1):171–179.

15. Ku G, Wang X, Stoica G, Wang LV. Multiple-bandwidth photoacoustic tomography. Phys Med Biol 2004;49(7):1329–1338.

16. Sessler GM. Piezoelectricity in polyvinylidenefluoride. J Acoust Soc Am 1981;70(6):1596.

17. Xia J, Yao J, Wang LV. Photoacoustic tomography: principles and advances. Electromagn Waves (Camb) 2014;147:1–22.

18. Jacques SL. Optical properties of biological tissues: a review. Phys Med Biol 2013;58(11):R37–R61.

19. Friebel M, Roggan A, Müller G, Meinke M. Determination of optical properties of human blood in the spectral range 250 to 1100 nm using Monte Carlo simulations with hematocrit-dependent effective scattering phase functions. J Biomed Opt 2006;11(3):34021.

20. Sethuraman S, Amirian JH, Litovsky SH, Smalling RW, Emelianov SY. Spectroscopic intravascular photoacoustic imaging to differentiate atherosclerotic plaques. Opt Express 2008;16(5):3362–3367.

21. Beard P. Biomedical photoacoustic imaging. Interface Focus 2011;1(4):602–631.

22. Allen TJ, Hall A, Dhillon AP, Owen JS, Beard PC. Spectroscopic photoacoustic imaging of lipid-rich plaques in the human aorta in the 740 to 1400 nm wavelength range. J Biomed Opt 2012;17(6):061209.

23. Wilson KE, Bachawal SV, Tian L, Willmann JK. Multiparametric spectroscopic photoacoustic imaging of breast cancer development in a transgenic mouse model. Theranostics 2014; 4(11):1062–1071. http://www.thno.org/v04p1062.htm. Accessed September 4, 2014.

24. Luke GP, Emelianov SY. Label-free detection of lymph node metastases with US-guided functional photoacoustic imaging. Radiology 2015;277(2):435–442.

25. Rich LJ, Seshadri M. Photoacoustic imaging of vascular hemodynamics: validation with blood oxygenation level-dependent MR imaging. Radiology 2015;275(1):110–118.

26. Wang X, Xie X, Ku G, Wang LV, Stoica G. Noninvasive imaging of hemoglobin concentration and oxygenation in the rat brain using high-resolution photoacoustic tomography. J Biomed Opt 2006;11(2):024015.

27. Kim JW, Dang CV. Cancer's molecular sweet tooth and the Warburg effect. Cancer Res 2006;66(18):8927–8930.

28. Cairns RA, Harris IS, Mak TW. Regulation of cancer cell metabolism. Nat Rev Cancer 2011;11(2):85–95.

29. Maeda H, Wu J, Sawa T, Matsumura Y, Hori K. Tumor vascular permeability and the EPR effect in macromolecular therapeutics: a review. J Control Release 2000; 65(1-2):271–284.

30. Prabhakar U, Maeda H, Jain RK, et al. Challenges and key considerations of the enhanced permeability and retention effect for nanomedicine drug delivery in oncology. Cancer Res 2013;73(8):2412–2417.

31. Luke GP, Yeager D, Emelianov SY. Biomedical applications of photoacoustic imaging with exogenous contrast agents. Ann Biomed Eng 2012;40(2):422–437.

32. Conde J, Doria G, Baptista P. Noble metal nanoparticles applications in cancer. J Drug Deliv 2012;2012:751075.

33. Eustis S, el-Sayed MA. Why gold nanoparticles are more precious than pretty gold: noble metal surface plasmon resonance and its enhancement of the radiative and nonradiative properties of nanocrystals of different shapes. Chem Soc Rev 2006;35(3):209–217.

34. Razansky D, Baeten J, Ntziachristos V. Sensitivity of molecular target detection by multispectral optoacoustic tomography (MSOT). Med Phys 2009;36(3):939–945.

35. Hannah A, Luke G, Wilson K, Homan K, Emelianov S. Indocyanine green-loaded photoacoustic nanodroplets: dual contrast nanoconstructs for enhanced photoacoustic and ultrasound imaging. ACS Nano 2014; 8(1):250–259.

36. Kim G, Huang SW, Day KC, et al. Indocyanine-green-embedded PEBBLEs as a contrast agent for photoacoustic imaging. J Biomed Opt 2007;12(4):044020.

37. Ashkenazi S. Photoacoustic lifetime imaging of dissolved oxygen using methylene blue. J Biomed Opt 2010;15(4):040501.

38. Song KH, Stein EW, Margenthaler JA, Wang LV. Noninvasive photoacoustic identification of sentinel lymph nodes containing methylene blue in vivo in a rat model. J Biomed Opt 2008;13(5):054033.

39. De la Zerda A, Zavaleta C, Keren S, et al. Carbon nanotubes as photoacoustic molecular imaging agents in living mice. Nat Nanotechnol 2008;3(9):557–562.

40. Wilson K, Homan K, Emelianov S. Biomedical photoacoustics beyond thermal expansion using triggered nanodroplet vaporization for contrast-enhanced imaging. Nat Commun 2012;3:618.

41. Strohm EM, Gorelikov I, Matsuura N, Kolios MC. Acoustic and photoacoustic characterization of micron-sized perfluorocarbon emulsions. J Biomed Opt 2012;17(9):96016–1.

42. Zackrisson S, van de Ven SM, Gambhir SS. Light in and sound out: emerging translational strategies for photoacoustic imaging. Cancer Res 2014;74(4):979–1004.

43. Yang X, Stein EW, Ashkenazi S, Wang LV. Nanoparticles for photoacoustic imaging. Wiley Interdiscip Rev Nanomed Nanobiotechnol 2009;1(4):360–368.

44. Oraevsky AA. Optoacoustic imaging of blood for visualization and diagnostics of breast cancer. Proc SPIE 2002;4618:81–94.

45. Bohndiek SE, Bodapati S, Van De Sompel D, Kothapalli SR, Gambhir SS. Development and application of stable phantoms for the evaluation of photoacoustic imaging instruments. PLoS One 2013;8(9):e75533.

46. Mallidi S, Luke GP, Emelianov S. Photoacoustic imaging in cancer detection, diagnosis, and treatment guidance. Trends Biotechnol 2011;29(5):213–221.

47. Kamaya A, Vaithilingam S, Chung BI, Oralkan O, Khuri-Yakub BT. Photoacoustic imaging of the bladder: a pilot study. J Ultrasound Med 2013;32(7):1245–1250.

48. Valluru KS, Chinni BK, Rao NA, Bhatt S, Dogra VS. Basics and clinical applications of photoacoustic imaging. Ultrasound Clin 2009;4(3):403–429.

49. Mehrmohammadi M, Yoon SJ, Yeager D, Emelianov SY. Photoacoustic imaging for cancer detection and staging. Curr Mol Imaging 2013;2(1):89–105.

50. Siegel R, Ma J, Zou Z, Jemal A. Cancer statistics, 2014. CA Cancer J Clin 2014;64(1): 9–29.

51. Berg WA, Blume JD, Cormack JB, et al. Combined screening with ultrasound and mammography vs mammography alone in women at elevated risk of breast cancer. JAMA 2008;299(18):2151–2163.

52. Skaane P, Bandos AI, Gullien R, et al. Comparison of digital mammography alone and digital mammography plus tomosynthesis in a population-based screening program. Radiology 2013;267(1):47–56.

53. Scheel JR, Lee JM, Sprague BL, Lee CI, Lehman CD. Screening ultrasound as an adjunct to mammography in women with mammographically dense breasts. Am J Obstet Gynecol 2015;212(1):9–17.

54. Hubbard RA, Kerlikowske K, Flowers CI, Yankaskas BC, Zhu W, Miglioretti DL. Cumulative probability of false-positive recall or biopsy recommendation after 10 years of screening mammography: a cohort study. Ann Intern Med 2011;155(8):481–492.

55. Brodersen J, Siersma VD. Long-term psychosocial consequences of false-positive screening mammography. Ann Fam Med 2013;11(2):106–115.

56. Kerlikowske K, Zhu W, Hubbard RA, et al. Outcomes of screening mammography by frequency, breast density, and postmenopausal hormone therapy. JAMA Intern Med 2013;173(9):807–816.

57. Piras D, Xia W, Steenbergen W, Van Leeuwen TG, Manohar S. Photoacoustic imaging of the breast using the Twente photoacoustic mammoscope: Present status and future perspectives. IEEE J Sel Top Quantum Electron 2010;16(4):730–739.

58. Heijblom M, Piras D, Xia W, et al. Visualizing breast cancer using the Twente photoacoustic mammoscope: what do we learn from twelve new patient measurements? Opt Express 2012;20(11):11582–11597.

59. Heijblom M, Piras D, Xia W, et al. Imaging breast lesions using the Twente Photoacoustic Mammoscope: ongoing clinical experience. In: Oraevsky AA, Wang LV, eds. Proceedings of SPIE: medical imaging 2012—photons plus ultrasound: imaging and sensing 2012. Vol 8223. Bellingham, Wash: International Society for Optics and Photonics, 2012; 82230C.

60. Ermilov SA, Khamapirad T, Conjusteau A, et al. Laser optoacoustic imaging system for detection of breast cancer. J Biomed Opt 2009;14(2):024007.

61. Ermilov SA, Fronheiser MP, Brecht HP, et al. Development of laser optoacoustic and ultrasonic imaging system for breast cancer utilizing handheld array probes. Proc SPIE 2009;7177:717703.

62. Lavin P, Ulissey MJ, Schoenfeld D, Stavros AT. Breast mass classification based on opto-acoustic features using data mining.

63. Stavros AT, Lerner A, Tucker L, Boyd B, Fine R, Burak W. Opto-acoustic imaging in the evaluation of BI-RADS 3 lesions: findings and implications. Natl Consort Breast Centers 2014. http://senomedical.com// images/ncbc%202014.pdf. Accessed June 24, 2015.

64. Kruger RA, Kuzmiak CM, Lam RB, Reinecke DR, Del Rio SP, Steed D. Dedicated 3D photoacoustic breast imaging. Med Phys 2013;40(11):113301.

65. Kitai T, Torii M, Sugie T, et al. Photoacoustic mammography: initial clinical results. Breast Cancer 2014;21(2):146–153.

66. Turner RR, Ollila DW, Krasne DL, Giuliano AE. Histopathologic validation of the sentinel lymph node hypothesis for breast carcinoma. Ann Surg 1997;226(3):271–276; discussion 276–278.

67. Harlow SP, Weaver DL. Sentinel lymph node biopsy in breast cancer: techniques. Waltham, Mass: UpToDate, 2013.

68. Kim C, Erpelding TN, Maslov K, et al. Handheld array-based photoacoustic probe for guiding needle biopsy of sentinel lymph nodes. J Biomed Opt 2010;15(4): 046010.

69. Erpelding TN, Kim C, Pramanik M, et al. Sentinel lymph nodes in the rat: noninvasive photoacoustic and US imaging with a clinical US system. Radiology 2010; 256(1):102–110.

70. Erpelding TN, Garcia-Uribe A, Krumholz A, et al. A dual-modality photoacoustic and ultrasound imaging system for noninvasive sentinel lymph node detection: preliminary clinical results. In: Oraevsky AA, Wang LV, eds. Proceedings of SPIE: medical imaging 2014—photons plus ultrasound: imaging and sensing 2014. Vol 8943. Bellingham, Wash: International Society for Optics and Photonics, 2014; 894359.

71. Luke GP, Myers JN, Emelianov SY, Sokolov KV. Sentinel lymph node biopsy revisited: ultrasound-guided photoacoustic detection of micrometastases using molecularly targeted plasmonic nanosensors. Cancer Res 2014;74(19):5397–5408.

72. Masuda H, Zhang D, Bartholomeusz C, Doihara H, Hortobagyi GN, Ueno NT. Role of epidermal growth factor receptor in breast cancer. Breast Cancer Res Treat 2012; 136(2):331–345.

73. Chan SK, Hill ME, Gullick WJ. The role of the epidermal growth factor receptor in breast cancer. J Mammary Gland Biol Neoplasia 2006;11(1):3–11.

74. Nicholson RI, Gee JM, Harper ME. EGFR and cancer prognosis. Eur J Cancer 2001;37(Suppl 4):S9–S15.

75. Esserman L, Shieh Y, Thompson I. Rethinking screening for breast cancer and prostate cancer. JAMA 2009;302(15):1685–1692.

76. Wang X, Roberts WW, Carson PL, Wood DP, Fowlkes JB. Photoacoustic tomography: a potential new tool for prostate cancer. Biomed Opt Express 2010;1(4):1117–1126.

77. Olafsson R, Bauer DR, Montilla LG, Witte RS. Real-time, contrast enhanced photoacoustic imaging of cancer in a mouse window chamber. Opt Express 2010;18(18): 18625–18632.

78. Bauer DR, Olafsson R, Montilla LG, Witte RS. 3-D photoacoustic and pulse echo imaging of prostate tumor progression in the mouse window chamber. J Biomed Opt 2011;16(2):026012.

79. Yaseen MA, Brecht HP, Ermilov SA, Gharieb RR, Conjusteau A, Oraevsky AA. Hybrid optoacoustic and ultrasonic imaging system for detection of prostate malignancies. Proc SPIE 2008;6856:68560T.

80. Yaseen MA, Ermilov SA, Brecht HP, et al. Optoacoustic imaging of the prostate: development toward image-guided biopsy. J Biomed Opt 2010;15(2):021310.

81. Agarwal A, Huang SW, O'Donnell M, et al. Targeted gold nanorod contrast agent for prostate cancer detection by photoacoustic imaging. J Appl Phys 2007;102(6):064701.

82. Levi J, Sathirachinda A, Gambhir SS. A high-affinity, high-stability photoacoustic agent for imaging gastrin-releasing peptide receptor in prostate cancer. Clin Cancer Res 2014;20(14):3721–3729.

83. Dogra VS, Chinni BK, Valluru KS, et al. Multispectral photoacoustic imaging of prostate cancer: preliminary ex-vivo results. J Clin Imaging Sci 2013;3:41.

84. Valluru KS, Chinni BK, Rao NA, Bhatt S, Dogra VS. Development of a c-scan photoacoustic imaging probe for prostate cancer detection. In: D'hooge J, Doyley MM, eds. Proceedings of SPIE: medical imaging 2011—ultrasonic imaging, tomography, and therapy. Vol 7968. Bellingham, Wash: Inter-

national Society for Optics and Photonics, 2011; 79680C.

85. Crook J. The role of brachytherapy in the definitive management of prostate cancer. Cancer Radiother 2011;15(3):230–237.

86. Nag S, Bice W, DeWyngaert K, Prestidge B, Stock R, Yu Y. The American Brachytherapy Society recommendations for permanent prostate brachytherapy postimplant dosimetric analysis. Int J Radiat Oncol Biol Phys 2000;46(1):221–230.

87. Lediju Bell MA, Kuo NP, Song DY, Kang J, Boctor EM. In vivo photoacoustic imaging of prostate brachytherapy seeds. In: Oraevsky AA, Wang LV, eds. In: Oraevsky AA, Wang LV, eds. Proceedings of SPIE: medical imaging 2014—photons plus ultrasound: imaging and sensing 2014. Vol 8943. Bellingham, Wash: International Society for Optics and Photonics, 2014; 894348.

88. Karakousis GC, Czerniecki BJ. Diagnosis of melanoma. PET Clin 2011;6(1):1–8.

89. Rigel DS, Russak J, Friedman R. The evolution of melanoma diagnosis: 25 years beyond the ABCDs. CA Cancer J Clin 2010;60(5):301–316.

90. Youl PH, Baade PD, Janda M, Del Mar CB, Whiteman DC, Aitken JF. Diagnosing skin cancer in primary care: how do mainstream general practitioners compare with primary care skin cancer clinic doctors? Med J Aust 2007;187(4):215–220.

91. Wolff T, Tai E, Miller T. Screening for skin cancer: an update of the evidence for the U.S. Preventive Services Task Force. Ann Intern Med 2009;150(3):194–198.

92. Staley J, Grogan P, Samadi AK, Cui H, Cohen MS, Yang X. Growth of melanoma brain tumors monitored by photoacoustic microscopy. J Biomed Opt 2010;15(4): 040510.

93. Galanzha EI, Shashkov EV, Spring PM, Suen JY, Zharov VP. In vivo, noninvasive, label-free detection and eradication of circulating metastatic melanoma cells using two-color photoacoustic flow cytometry with a diode laser. Cancer Res 2009;69(20):7926–7934.

94. McCormack D, Al-Shaer M, Goldschmidt BS, et al. Photoacoustic detection of melanoma micrometastasis in sentinel lymph nodes. J Biomech Eng 2009;131(7): 074519.

95. In vivo real-time detection of circulating melanoma cells. https://clinicaltrials.gov/ct2/show/NCT01776905. Accessed June 26, 2015.

96. Jose J, Grootendorst DJ, Vijn TW, et al. Initial results of imaging melanoma metastasis in resected human lymph nodes using photoacoustic computed tomography. J Biomed Opt 2011;16(9):096021.

97. Zhou Y, Xing W, Maslov KI, Cornelius LA, Wang LV. Handheld photoacoustic microscopy to detect melanoma depth in vivo. Opt Lett 2014;39(16):4731–4734.

98. Langhout GC, Grootendorst DJ, Nieweg OE, et al. Detection of melanoma metastases in resected human lymph nodes by noninvasive multispectral photoacoustic imaging. Int J Biomed Imaging 2014;2014: 163652.

99. Favazza CP, Jassim O, Cornelius LA, Wang LV. In vivo photoacoustic microscopy of human cutaneous microvasculature and a nevus. J Biomed Opt 2011;16(1):016015.

100. Mandel SJ, Langer JE, Duick DS. Ultrasound of thyroid nodules. In: Baskin HJ, Duick DS, Levine RA, eds. Thyroid ultrasound and ultrasound-guided FNA. 2nd ed. New York, NY: Springer Science+Business Media, 2008; 77–95.

101. Wong KT, Ahuja AT. Ultrasound of thyroid cancer. Cancer Imaging 2005;5:157–166.

102. Rago T, Vitti P. Role of thyroid ultrasound in the diagnostic evaluation of thyroid nodules. Best Pract Res Clin Endocrinol Metab 2008;22(6):913–928.

103. Virmani V, Hammond I. Sonographic patterns of benign thyroid nodules: verification at our institution. AJR Am J Roentgenol 2011;196(4):891–895.

104. Popoveniuc G, Jonklaas J. Thyroid nodules. Med Clin North Am 2012;96(2):329–349.

105. Suster S. Thyroid tumors with a follicular growth pattern: problems in differential diagnosis. Arch Pathol Lab Med 2006;130(7):984–988.

106. Levi J, Kothapalli SR, Bohndiek S, et al. Molecular photoacoustic imaging of follicular thyroid carcinoma. Clin Cancer Res 2013;19(6):1494–1502.

107. Kobayashi H, Choyke PL. Target-cancer-cell-specific activatable fluorescence imaging probes: rational design and in vivo applications. Acc Chem Res 2011;44(2): 83–90.

108. Dogra VS, Chinni BK, Valluru KS, et al. Preliminary results of ex vivo multispectral photoacoustic imaging in the management of thyroid cancer. AJR Am J Roentgenol 2014;202(6):W552–W558. 109. American Cancer Society. Cancer facts & figures 2015. Atlanta, Ga: American Cancer Society, 2015.

110. Lutz AM, Willmann JK, Drescher CW, et al. Early diagnosis of ovarian carcinoma: is a solution in sight? Radiology 2011;259(2): 329–345.

111. Buys SS, Partridge E, Black A, et al. Effect of screening on ovarian cancer mortality: the Prostate, Lung, Colorectal and Ovarian (PLCO) Cancer Screening Randomized Controlled Trial. JAMA 2011;305(22): 2295–2303.

112. Aguirre A, Ardeshirpour Y, Sanders MM, Brewer M, Zhu Q. Potential role of coregistered photoacoustic and ultrasound imaging in ovarian cancer detection and characterization. Transl Oncol 2011;4(1): 29–37.

113. Kumavor PD, Alqasemi U, Tavakoli B, et al. Co-registered pulse-echo/photoacoustic transvaginal probe for real time imaging of ovarian tissue. J Biophotonics 2013;6(6-7): 475–484.

114. Alqasemi U, Li H, Yuan G, Aguirre A, Zhu Q. Ultrafast ultrasound and photoacoustic co-registered imaging system based on FPGA parallel processing. In: Oraevsky AA, Wang LV, eds. Proceedings of SPIE: medical imaging 2012—photons plus ultrasound: imaging and sensing 2012. Vol 8223. Bellingham, Wash: International Society for Optics and Photonics, 2012; 82232U.

115. Peng K, He L, Wang B, Xiao J. Detection of cervical cancer based on photoacoustic imaging-the in-vitro results. Biomed Opt Express 2015;6(1):135–143.

116. Petrov A, Prough DS, Petrov IY, et al. Cerebral venous blood oxygenation monitoring during hyperventilation in healthy volunteers with a novel optoacoustic system. In: Oraevsky AA, Wang LV, eds. Proceedings of SPIE: medical imaging 2013—photons plus ultrasound: imaging and sensing 2013. Vol 8581. Bellingham, Wash: International Society for Optics and Photonics, 2013; 85814Z.

117. Yang JM, Maslov K, Yang HC, Zhou Q, Wang LV. Endoscopic photoacoustic microscopy. SPIE BiOS Biomed Opt 2009;7177:71770N.

118. O'Brien CM, Rood K, Sengupta S, et al. Detection and isolation of circulating melanoma cells using photoacoustic flowmetry. J Vis Exp 2011 (57):e3559.

119. Weight RM, Dale PS, Viator JA. Detection of circulating melanoma cells in human blood using photoacoustic flowmetry. Conf Proc IEEE Eng Med Biol Soc 2009;2009:106–109.

120. Wang B, Yantsen E, Sokolov K, Emelianov S. High sensitivity intravascular photoacoustic imaging of macrophages. Proc SPIE 2009; 7177:71770V.

121. Tavakolian P, Kosik I, Chamson-Reig A, et al. Potential for photoacoustic imaging of the neonatal brain. Proc SPIE 2013;8581: 858146.

122. Wang X, Chamberland DL, Xi G. Noninvasive reflection mode photoacoustic imaging through infant skull toward imaging of neonatal brains. J Neurosci Methods 2008;168(2):412–421.

123. Wu N, Ye S, Ren Q, Li C. High-resolution dual-modality photoacoustic ocular imaging. Opt Lett 2014;39(8):2451–2454.

124. LOUIS-3D Breast Study. https://clinicaltrials.gov/ct2/show/NCT01755130. Accessed June 26, 2015.

125. The PIONEER-01 Pivotal Study of the Imagio Breast Imaging System. https://clinicaltrials.gov/ct2/show/NCT01943916. Accessed June 26, 2015.

126. Simulated Screening Study for Breast Imaging. https://clinicaltrials.gov/ct2/show/NCT01807754. Accessed June 26, 2015.

127. Breast imaging using light and sound. http://www.trialregister.nl/trialreg/admin/rctview.asp?TC=2945. Accessed June 26, 2015.

128. Photoacoustic tomography (PAT) in combination with high resolution ultrasound for non-invasive diagnosis of sentinel lymph node in patients with malignant melanoma. http://apps.who.int/trialsearch/Trial2.aspx?TrialID=DRKS00005447. Accessed June 26, 2015.

129. Photoacoustic Imaging (PAI) of the Prostate. A Clinical Feasibility Study. https://clinicaltrials.gov/ct2/show/NCT01551576. Accessed June 26, 2015.

130. Visualization of Rectal Cancer During Endoscopy, Using a Fluorescent Tracer (RAPI-DO-TRACT). https://clinicaltrials.gov/ct2/show/NCT01972373. Accessed June 26, 2015.

131. Stavros AT, Lerner A, Burak W, et al. Opto-acoustic breast imaging, a new technology. Natl Consort Breast Centers 2013. http://senomedical.com/images/stories/posters_2013/NCBC_2013.pdf. Accessed June 24, 2015.

132. Twente Photoacoustic Mammoscope May Lead to Radiation-Free Breast Cancer Screening. http://www.medgadget.com/2012/06/twente-photoacoustic-mammoscope-may-lead-to-radiation-free-breast-cancer-screening.html. Published 2012. Accessed June 29, 2015.

133. Kitai T, Kyoto J. Clinical development of photoacoustic mammography for the diagnosis of breast cancer. Eur Congr Radiol 2012.